(MSS) membranes". *Journal of Membrane Science*, **v229**, pp 229-235 (2007).

Flowfields on feed and Permeate sides of Tubular Molecular Sieving Silica (MSS) Membranes

M.M Abdel-jawad[1] *, S. Gopalakrishnan*[1]*, M.C. Duke*[1]*, M.N. Macrossan*[2] *, P. Smith Schneider*[3]*, J.C. Diniz da Costa*[1]

[1]FIMLab – Films and Inorganic Membrane Laboratory, Division of Chemical Engineering, and [2]Division of Mechanical Engineering, School of Engineering, The University of Queensland, Qld 4072 Australia, [3]Department of Mechanical Engineering, Universidade Federal do Rio Grande do Sul, Porto Alegre, RS , 90050-170 Brazil

Keywords: Gas separation, Molecular Sieving Silica, Membranes, membrane flow CFD

Abstract

We present a novel Computational Fluid Dynamic approach to integrate diffusion through inorganic Molecular Sieve Silica (MSS) membranes and continuum flows on the feed/retentate and permeate sides of these membranes. In this approach, we model the membrane by creating a bounded region separating the feed/retentate side from the permeate side in which only the phenomenological equations of the activated gas transport model apply. Continuum flows on both sides of this region are described by the Navier-Stokes equations and gas-through-gas diffusion is modeled using the Stefan-Maxwell model only. The phenomenological equations are applicable exclusively to diffusion through the membrane. By coupling these equations we obtain complete flowfields on the feed/retentate and permeate sides of

---

MSS membranes. The complete model characterizes the flow of CO, CO_2, He, H_2, and N_2 and gas mixtures of CO_2 and H_2 on both sides of tubular MSS membranes and is validated by comparing flow rates with single gas experiments. We found that partial pressure axial distributions in the feed/retentate and permeate streams of the membrane are constant. In the permeate stream, the radial variation of axial velocity across the flow is nearly the same for all axial locations. There is a linear increase of axial velocity (and total flow rate) with axial coordinate.

1. Introduction

Clean energy delivery systems, such as coal gasification, which produce H_2 can significantly reduce the adverse environmental impact of greenhouse gases if CO_2 is captured and subsequently stored. There is, however, a need to separate H_2 from CO_2 at temperatures above 200^{o}C which can be met by inorganic membrane technologies. As an example, the ultramicropores (~3Å) of amorphous silica are suitably sized for sieving the small H_2 (d_k=2.89 Å) molecules from larger CO_2 (d_k=3.3 Å) molecules. When amorphous silica is applied as a film of thickness 10-100 nm on top of porous substrates, a 'molecular sieve' is formed resulting in activated transport and achieving high selectivity of H_2 over CO_2 and high flow rates [1, 2].

Figure 1 shows a schematic view of a membrane system employing a tubular arrangement to separate gases. The feed inlet stream contains a gas mixture (unseparated gases) which requires processing provided by the membrane. There are two outlet streams: the permeate stream, which is composed of the purified gas processed through the membrane and the retentate stream, which is composed of the gases which have not passed through the membrane. Flow rates and hence Reynolds numbers are typically low for this type of system, and the flow is therefore expected to be laminar. The system is axisymmetric and therefore, only a plane bounded by the axis of symmetry need be modelled for single tube systems.

The effect of microscopic gaseous flow through MSS membranes on the macroscopic flow parameters

---

in both permeate and feed/retentate streams has up till now not been known; only experimental measurements of the bulk flow rates have been made. In this regard, there is no agreement in the literature where four different assumed axial distributions of driving pressure ΔPi across the membrane have been proposed. These profiles include (i) the partial pressure difference between at the feed inlet and the permeate outlet [3], (ii) the partial pressure difference between retentate and the permeate outlets [4-7], (iii) a logarithmic axial distribution of partial pressure along the membrane, which can be expressed in terms of either partial pressure αP or concentration of both species [8-10], and (iv) the average partial pressure on the source side, analogous to solving the differential mass balance in a 1D approach has been used [11]. Different flow results can be derived depending on the assumed profiles of ΔPi used in the simulation of gas fields. In turn, this has serious implications for an industrial design application, where the retentate is flushed from the system to preserve the mole fraction of the gas to be separated and maintain the performance of the gas separation system.

Computational fluid dynamics has previously been applied to membranes in systems to separate liquid components [12-14] and the field is extensively reviewed by Ghidossi et al. [15]. There is limited literature reported on CFD modelling of gas separation membranes [16, 17, 18]. Bao and Lipscomb [16, 17]] have used computational techniques to analyse flows on one side of hollow fiber membranes, while Takaba and Nakao [18] used the software package PHOENICS to simulate the permeation of CO/H_2 mixtures through the membrane. Concentration polarisation was reported in the boundary layer on the feed/retentate side of the membrane [18].

Microporous membranes preclude continuum flow through them which presents a challenge to conventional Navier-Stokes solvers. In the case of MSS membranes, single gas diffusion within the ultramicropores is governed by an activated transport mechanism originally described by Barrer in the

---

early 1940s [19]. Thus adsorption and mobility energy in silica ultramicropores play a significant role in gas diffusion, though it is generally reported that gas adsorption to the silica surface follows Henry's law [2, 20-22]. Nevertheless, there is no CFD work reported in the literature modelling of gas-through-gas diffusion through membrane systems where interaction adsorption and mobility energy is taken into account.

In this work, we are concerned with complete characterisation of the flow fields on the feed/retentate and permeate sides of membranes allowing for gas-through-gas diffusion on both sides of the membrane as well as diffusion through the ultramicropores of the membrane. We use the Navier-Stokes equations to describe flows on both sides of the membrane and only account for gas-through-gas diffusion using the Stefan Maxwell diffusion model. We describe diffusion through the membranes using only the phenomenological equations of the activated transport model. The ability to characterise flowfields on the feed/retentate and permeate sides of membranes enables us to isolate flow effects on membrane performance. We present the technique and validate the results with experiments for single gas runs and extend the simulations to mixed gases to show typical flowfields and their characteristic pressure and velocity fields. In addition, we also investigate the pressure difference profile across the membrane.

2. Methods

In the feed/retentate (source) and permeate (sink) regions of the membrane, concentration driven flux *j* of species *i* can be stated [23] as

$$j_i = -\rho D_i \nabla Y \qquad \text{Eq. 1}$$

where the diffusivity *Di* is calculated as

$$Di = \frac{1 - X_i}{\sum_{j=1}^{n} \frac{X_j}{D_{ij}}} \qquad \text{Eq. 2}$$

---

and

$$D_{ij} = 0.018583 \frac{T^{\frac{3}{2}} \sqrt{\frac{1}{M_i} + \frac{1}{M_j}}}{P\sigma_{ij}^{\,2} \frac{k}{\sqrt{\varepsilon_i \varepsilon_j}}} \qquad \text{Eq. 3}$$

where σ is the Lennard-Jones collision diameter, k is Boltzmann's constant and $\sqrt{\varepsilon_i \varepsilon_j}$ is the characteristic energy of interaction, . The Stefan-Maxwell equations are used to ensure that the total concentration is always $\sum_{i=1}^{n} Y_i = 1.0$. This is especially important in multi-component species gas mixtures [24].

Equations 1-3 are applied only to model the gas phase on the feed/retentate and permeate sides of the membrane. The membrane is modeled using only the phenomenological equation (Eq. 4). Convection and gas-through-gas diffusion using the Stefan-Maxwell model are modeled using CFD-ACE which is a commercial finite volume Navier-Stokes solver. This simulation is only interfered with for the transfer of mass, momentum and energy transfer across the boundaries on the feed/retentate and permeate regions between which the membrane resides. The operation of the membrane is described using an external code that couples the phenomenological equation (Eq. 4) to the Navier-Stokes solver and the Stefan-Maxwell diffusion model.

In this work we used MSS Membranes manufactured according to a standard procedure reported elsewhere [25]. Silica coated tubular membranes were deposited on alumina substrates of 10mm diameter, 80mm axial length supplied by Noritake and installed into a single tube test module similar to the schematic in Figure 1. The alumina substrate provides the mechanical strength required for the membrane system. The alumina substrate has large pores (~d_p = 500 nm), allowing for low resistance to gas flux. On the other hand, the top silica layer has pores in the molecular sieve range (d_p<0.5nm), which is the limiting factor for mass transfer from the feed side to the permeate side [20, 25]. Membrane

---

permeances were determined using a bubble meter to measure the flow rates at temperatures between 100-450^{o}C with an estimated experimental variance of 4%. The permeance data from single gas experiments were used to find the best fit values of the constants $C_{0,i}$ and $E_{a,i}$ in the activated transport model [2, 20-22]

$$\frac{P_i}{l} = \frac{\rho_{silica}}{l}\frac{1-\varepsilon}{\varepsilon} D_{0,i} K_{0,i} \exp\left(\frac{-E_{a,i}}{RT}\right) = C_{0,j} \exp\left(\frac{E_{a,j}}{RT}\right) \qquad \text{Eq. 4}$$

In Eq. 5, i denotes the species, $\frac{P_i}{l}$ the permeance (mol.m^{-2}.s^{-1}.Pa^{-1}), ρ_{silica} is the silica density (kg.m^{-3}), ε is the silica porosity (-), $D_{0,i}$ is the diffusivity coefficient (m^2.s^{-1}), $K_{0,i}$ is the Henry's constant (mol.kg^{-1}.Pa^{-1}), $E_{a,i}$ is the transport activation energy (kJ.kmol^{-1}), R is the universal gas constant (8.314 kJ.kmol^{-1}.K^{-1}) and T is the membrane temperature (K). The pre-exponential multipliers have been lumped together as $C_{0,i}$.,. Values of $C_{0,i}$ and $E_{a,i}$ for each species i are shown in Table 1. The values in table 1 are of the same order of magnitude as in previous papers [9, 20, 25]. These values were obtained from single gas permeation tests using a bubble meter to measure the permeate flow while the retentate stream was at a dead end mode. The feed pressures, temperature and concentrations and the outlet pressures are set in the simulation to match the experiments. The simulation outputs flow rates and concentrations in the retentate and permeate sides as well as complete field distributions of velocities, pressures and densities for both sides of the tube.

The problem was then set up computationally using a structured grid and a commercial finite volume compressible flow solver (CFD-ACE). Single gas cases were run with fixed pressures set at the feed inlet as well as the retentate and permeate outlets. The boundary separating the feed/retentate side from the permeate side was designated a no slip wall but a specially written Fortran-90 user subroutine was allowed to interrupt the solver for every boundary cell at every time step in order to transfer the mass, momentum and energy of the permeating species from the source to the sink side of the membrane. It was assumed that the mass flow through the membrane was in the radial direction only. The temperature

---

and partial pressures on both side of the membrane surface were determined and Eq. 4 (with values from Table 1) was used to determine the permeance for each species. The product of the permeance with cell interface area and the difference in partial pressure in the radial direction across the membrane gave the mass flow of each species across these boundary cells. The appropriate amounts of mass, momentum and energy were then transferred between the cells on either side of the membrane.

After validating the performance of the model using single gas tests and simulations, we conducted mixed gas simulations using the binary mixture of CO_2 and H_2 to investigate the partial pressure flowfields in the flow regions on the feed/retentate and permeate sides of a molecular sieving membrane. Simulations modeled the CO_2/H_2 binary gas flow system at temperatures of 100^{o}C, 200^{o}C, 300^{o}C, 400^{o}C and 450^{o}C and with a pressure difference of one atmosphere across the membrane to ensure the flow regime remains within Henry's Law. A feed mixture containing mole fractions of CO_2 and H_2 of 0.5 was used for all simulations.

3. Results

Figure 2 shows the flow rates obtained from single gas simulations, compared with those measured from experiments at the same conditions. The simulated and measured flow rates agree to within five percent; the differences can be attributed to the experimental error in measurement which was estimated at the same percentage. Based on the permeances through the membrane and a membrane thickness of 120nm we find that diffusivities on the feed/retentate and permeate sides of the membrane are about 4 orders of magnitude greater than those through the membrane. This indicates gas-through-gas diffusion on the feed/retentate and permeate sides of the membrane occurs at a much faster rate than through the membrane. It is this characteristic of flow on the feed/retentate and permeate sides of membranes that differs from heat conduction in isotropic materials and hence hints at the inapplicability of a logarithmic distribution of partial pressures in the axial direction. Figure 3 shows the pressure distributions near the

membrane on both the feed side and the permeate side for a single gas simulation. It can be seen that the pressures on both sides of the membrane are near constant along the length of the membrane. There is no constraint in the methodology of these simulations that prescribes a constant pressure along the membrane. Hence even though pressure differences along the length of the membrane are prescribed by discretised incremental diffusion through the membrane and we find that there is little variation in pressure with axial coordinate. The boundary conditions on the permeate and retentate outlets in these simulations was a standard constant pressure outlet. In this type of outlet, the back pressure is specified by the user and all other variables are calculated by the code. This is the only appropriate condition to model an entire tube. Since the experiments were conducted using a bubble meter which is open to the atmosphere, the outlet pressure was prescribed to be at one atmosphere. Since the gas outside the membrane does not have a radial velocity, there is a drop in the radial velocity towards the outlet. All boundary conditions are shown in figure 2.

At constant temperature, this pressure field prescribes a near constant density field in the feed and permeate regions separately. This allows conservation of mass to prescribe a near constant radial velocity with axial coordinate on both sides of the membrane except near the no-slip end-walls, where all velocities are zero, and at the outlet, where velocity is purely axial. These edge effects can be seen as spikes in the radial velocity plots as a function of axial coordinate near x = 0 and x = 0.08 m in Figure 3 along the feed-membrane interface region and the substrate-permeate interface as the only axial variation of radial velocity (lines bounded by '+' signs in figure). Figure 3 shows that this is true of the axial velocity flowfield as a whole while there is obvious significant radial acceleration with radial coordinate as a result of the radial flow convergence process.

Figure 4 shows a typical axial velocity field, and a plot of the parameter $\eta = r/r_{tube}$, where r_{tube} is the radius of the tube, against the non-dimensional axial flow velocity $\zeta = \pi\, r_{tube}^2\, U/(2Q_x)$. Here $Q_x = x/L_{tube}$

Q, is the nominal volumetric flow rate through the membrane up to station x, L_{tube} is the total length of the membrane and Q is the predicted total flow rate through the membrane given by $Q = (P/l)\Delta P (2\pi r_{tube}L_{tube})/(M/\rho)$. Here ΔP is the difference in pressure between the feed inlet and the permeate outlet, ρ the density in the permeate. Velocity profiles are shown for x equal to $0.2\ L_{tube}$, $0.4\ L_{tube}$, $0.6\ L_{tube}$ and $0.8\ L_{tube}$ and M is the molecular mass of the relevant species (in this case Hydrogen).

The curves at the four locations nearly collapse onto the parabolic analytical solution of the Navier-Stokes equation for pipe flow given by $\zeta = 1 - \eta^2$ indicating near self-similarity. The numerical results slightly differ from the analytical solution of the Navier-Stokes equation for axial pipe flow because the flow enters the permeate region radially and also leaves the feed region radially in these simulations. Note that the volumetric flow rate Q_x within the parameter ζ is proportional to the length of the tubular membrane, so that a constant value of the non-dimensional velocity indicates that the axial velocity increases linearly from left (where the tube is blocked and $L = 0$) to right (where the permeate outlet is located). This occurs by virtue of mass conservation due to the tube being prismatic (see sections *A-A* and *B-B* in figure 6).

Figure 5 shows partial pressure differences along the normalised x-coordinate in the source for the mixed gas simulations. . Axial and radial velocity distributions for these simulations were similar to the single gas simulations seen in Figure 3 and Figure 4. It can be seen from Figure 5 that the driving pressure for H_2 decreases with increasing temperature while that for CO_2 increases with increasing temperature. Nevertheless the partial pressure differences along the axial coordinate and hence the concentration gradients are near constant and are around the levels of the feed. This was also the case for the first set of simulations where the composition of the retentate outlet was set to be pure N_2. This is to be expected as the diffusivity of each species in the on the feed/retentate and permeate sides of the membrane in the source and sink regions is far greater than that through the membrane and the highly mobile H_2 quickly replenishes any changes in concentration that have occurred due to selective diffusion

---

through the membrane. Other researchers [26], when considering flow through membranes, have used the assumption that the gas phase on both sides of the membrane is well mixed. This would be supported in cases such as the one presented here where rate of diffusion of gas through gas is greater than that of gas through the membrane. Recently however, membranes have been described in the literature where the flow rates through these membranes is exceptionally high [27]. Flows through these membranes may induce significant concentration polarisation and a large axial concentration gradients in contradistinction to the cases described here.

4. Conclusions

Flow fields on the feed/retentate and permeate sides of tubular MSS membranes have been studied. The Stefan-Maxwell and Navier-Stokes equations are used to describe only the gas phase regions on the feed/retentate and permeate sides. The phenomenological equations are used exclusively to describe the permeation through the membrane. Single gas simulations provided similar axial and radial velocity fields and results were validated with experimental data. . This work showed that, for typical operation of systems employing MSS membranes, the diffusion of gas species through the membrane is slow compared to diffusion in the gas either side of the membrane. This along with the fact that the dynamic pressure of the flow is negligible compared to the static pressure, results in uniform partial pressure axial distributions on both the feed/retentate and permeates streams of the membrane. The flow is nearly that of self-similar flow in pipes i.e. the radial variation of axial velocity across the flow is nearly the same for all axial locations. Further, there is a linear increase of axial velocity (and total flow rate) with axial coordinate. Mixed gas simulations provided the same axial and radial velocity fields and showed no variation of partial pressure along the axial coordinate of the membranes.

Author's version of M. M Abdel-jawad , S. Gopalakrishnan, M. C. Duke, M. N. Macrossan, P. Smith Schneider, J. C. Diniz da Costa "Flowfields on feed and permeate sides of tubular Molecular Sieving Silica (MSS) membranes". *Journal of Membrane Science*, **v229**, pp 229-235 (2007).

References

1. Uhlhorn, R.J.R., Keizer, K. , Burggraaf, A. J., Gas Transport And Separation With Ceramic Membranes. Part II. Synthesis And Separation Properties Of Microporous Membranes. Journal Of Membrane Science, 66 (1992.): 271.
2. de Vos, R.M., Verweij, H., Improved Performance Of Silica Membranes For Gas Separation. Journal Of Membrane Science, 143 (1998.): 37.
3. Lababidi, H., Al-Enezi, G. A. Ettouney, H. M., Optimization Of Module Configuration In Membrane Gas Separation. Journal Of Membrane Science, 112 (1996.): 185.
4. Tessendorf, S., R.Gani & Michelsen, M. L., Modeling, Simulation And Optimization Of membrane-Based Gas Separation Systems. Chemical Engineering Science, 54 (1999.): 943.
5. Corti, A., Fiaschi, D. , Lombardi, L., Carbon Dioxide Removal In Power Generation Using Membrane Technology. Energy, 29 (2004.): 2025.
6. Ettouney, H.M., Al-Enezi, G. , Hughes, R., Modelling Of Enrichment Of Natural Gas Wells By Membranes. Gas Separation & Purification, 9 (1995.): 3.
7. Conesa, A., A. Fernandez Roura, J.A. Pitarch, I. Vicente-Mingarro, M.A. Rodriguez, Separation Of Binary Gas Mixtures By Means Of Sol-Gel Modified Ceramic Membranes. Prediction Of Membrane Performance. Journal Of Membrane Science, 155 (1999.): 123.
8. Pettersen, T.,K.M. Lien, Design Studies Of Membrane Permeator Processes For Gas Separation. Gas Separation & Purification, 9 (1995.): 151.
9. Duke, M.C., D.d.C.J. C., G.Q. Lu, Modeling Hydrogen Separation In High Temperature Silica Membrane Systems. . Aiche Journal, 52 (2006.): 1729.
10. Sjardin, M., K.J. Damen, A.P.C. Faaij, Techno-Economic Prospects Of Small-Scale Membrane Reactors In A Future Hydrogen-Fuelled Transportation Sector. Energy, 31 (2006.): 2523.
11. Bounaceur, R., N. Lape, D. Roizard, C. Vallieres, E. Favre, Membrane Processes For Post-Combustion Carbon Dioxide Capture: A Parametric Study. Energy, 31 (2006.): 2556.
12. Marriott, J., E. Sorensen, I.D.L. Bogle, Detailed mathematical modelling of membrane modules. Comput. Chem. Eng., 25 (2001.): 693–700.
13. Willey, D.,D.F. Fletcher, Computational fluid dynamics modeling of flow and permeation for pressure-driven membrane processes. Desalination, 145 (2002.): 183.
14. Huang, L.,M.T. Morrissey, Finite element analysis as a tool for crossflow membrane filter simulation. J. Membr. Sci. 155, 155 (1999.): 19–30.
15. Ghidossi, R., D. .Veyret, P. Moulin, Computational fluid dynamics applied to membranes: State of the art and opportunities. Chemical Engineering and Processing, 45 (2006.): 437–454.
16. Bao, L.,G.G. Lipscomb, Effect of random fiber packing on the performance of shell-fed hollow fiber gas separation modules. Desalination, 146 (2002.): 243.
17. Lipscomb, G.G.,S. Sonalkar, Sources of Non-ideal Flow Distribution and Their Effect on the Performance of Hollow Fiber Gas Separation Modules. Separation & Purification Reviews, 33 (2005.): 41.
18. Takaba, H.,S. Nakao, Computational fluid dynamics study on concentration polarization in H2/CO separation membranes. Journal of Membrane Science, 249 (2005.): 83.
19. Barrer, R.M., Diffusion In And Through Solids. 1941: Cambridge University Press, University Of Cambridge, UK.
20. Diniz da Costa, J.C.D., G.Q.M. Lu, V. Rudolph, Y.S. Lin, Novel molecular sieve silica (MSS) membranes: characterisation and permeation of single-step and two-step sol-gel membranes. Journal of Membrane Science, 198 (2002.): 9.
21. de Lange, R.S.A., Hekkink, J. H. A., Keizer, K. , Burggraaf, A. J., Permeation And Separation Studies On Microporous Sol-Gel Modified Ceramic Membranes. Microporous Materials, 4 (1995.): 169.
22. Burggraaf, A.J., Single Gas Permeation Of Thin Zeolite (Mfi) Membranes: Theory And Analysis Of Experimental Observations. Journal Of Membrane Science, 155 (1999.): 45.
23. CFD-ACE+™ V2004 Modules Manual - Volume 1 Revision Date: May 1, 2004.
24. Duncan, J.B.,H.L. Toor, An experimental study of three component gas diffusion. AIChE Journal, 8 (1962.): 38.
25. Duke, M.C., Diniz Da Costa, J. C., Lu, G. Q. (Max), Petch, M. & Gray, P., Carbonised Template Molecular Sieve Silica Membranes In Fuel Processing Systems: Permeation, Hydrostability And Regeneration. Journal Of Membrane Science, 241 (2004.): 325.
26. Skoulidas, A.,D. Sholl, Multiscale Models of Sweep Gas and Porous Support Effects on Zeolite Membranes. AIChe Journal, 51 (2005.): 867.
27. Holt, J.K., et al., Fast Mass Transport Through Sub–2-Nanometer Carbon Nanotubes. Science, 312 (2006.): 1034.

Author's version of M. M Abdel-jawad , S. Gopalakrishnan, M. C. Duke, M. N. Macrossan, P. Smith Schneider, J. C. Diniz da Costa "Flowfields on feed and permeate sides of tubular Molecular Sieving Silica (MSS) membranes". *Journal of Membrane Science*, **v229**, pp 229-235 (2007).

Acknoledgment

The authors acknowledge financial support by the Centre for Low Emission Technology (www.clet.net) in Australia.

Author's version of M. M Abdel-jawad , S. Gopalakrishnan, M. C. Duke, M. N. Macrossan, P. Smith Schneider, J. C. Diniz da Costa "Flowfields on feed and permeate sides of tubular Molecular Sieving Silica (MSS) membranes". *Journal of Membrane Science*, **v229**, pp 229-235 (2007).

Nomenclature

A	surface area	m^2
$D_{0,i}$	diffusivity coefficient	$(m^2.s^{-1})$
d_k	*molecular kinetic diameter*	*(Å)*
dp	*pore diameter*	
$E_{a,i}$	Transport activation energy	$(kJ.kmol^{-1})$
$K_{0,i}$	Henry's constant	$(mol.kg^{-1}.Pa^{-1})$
l , L	axial length	(m)
$\dot{n}_i$	molar flow rate	kmol/s
n	number of species	
P	Pressure	(Pa)
$(P/l)_i$	membrane permeance	$kmol\ kPa^{-1}\ m^{2-1}\ s^{-1}$
ΔP_i	pressure drop	kPa
R	Universal gas constant	$(8.314\ kJ.kmol^{-1}.K^{-1})$
r	radius	(m)
T	Temperature	(K)
X	mole fraction	
Y	mass fraction	
ρ	density	$(kg.m^{-3})$
x	axial position	
ε	porosity	
σ	Lennard-Jones collision diameter	(m)
$\sqrt{\varepsilon_i \varepsilon_j}$	Characteristic energy of interaction.	
k	Boltzmann's constant	

Subscript

i	species or component
f	feed
h	high
l	low
p	permeate
r	retentate
s	sweep
tube	tube

List of Tables

Table 1: Fitting parameters for Equation 1 used in CFD modelling.

List of Figures

Figure 1 Schematic of a system to separate gases

Figure 2 Schematic representation of the numerical problem

Figure 3 Comparison of flow rates from single gas simulations with experimental measurements (Note CO flow rate multiplied by 2 to separate CO curves from N_2 curves on the graph)

Figure 4 (Lower) Radial velocity field. (Upper) Pressure and Radial velocity as a function of axial coordinate. Simulation for pure H_2 flow at 400^{o}C. Flowfield stretched in the radial direction by a factor of 3 for better visibility.

Figure 5 Axial velocity distributions as a function of radial coordinate on the sink side. Simulation for pure H_2 flow at 400^{o}C.

Figure 6 Partial pressure differences ΔPi across the membrane along the normalized axial coordinate, for mixed gas simulations (CO_2/H_2)

Table 1: Fitting parameters for Equation 1 used in CFD modelling.

Gas species i	$C_{0,i}$	$E_{a,i}$
	($mol.m^{-2}.s^{-1}.Pa^{-1}$)	($kJ.mol^{-1}$)
He	5.11×10^{-6}	10.19
H_2	2.72×10^{-6}	8.78
CO_2	3.29×10^{-8}	-1.72
N_2	4.62×10^{-8}	3.55
CO	7.06×10^{-8}	5.33

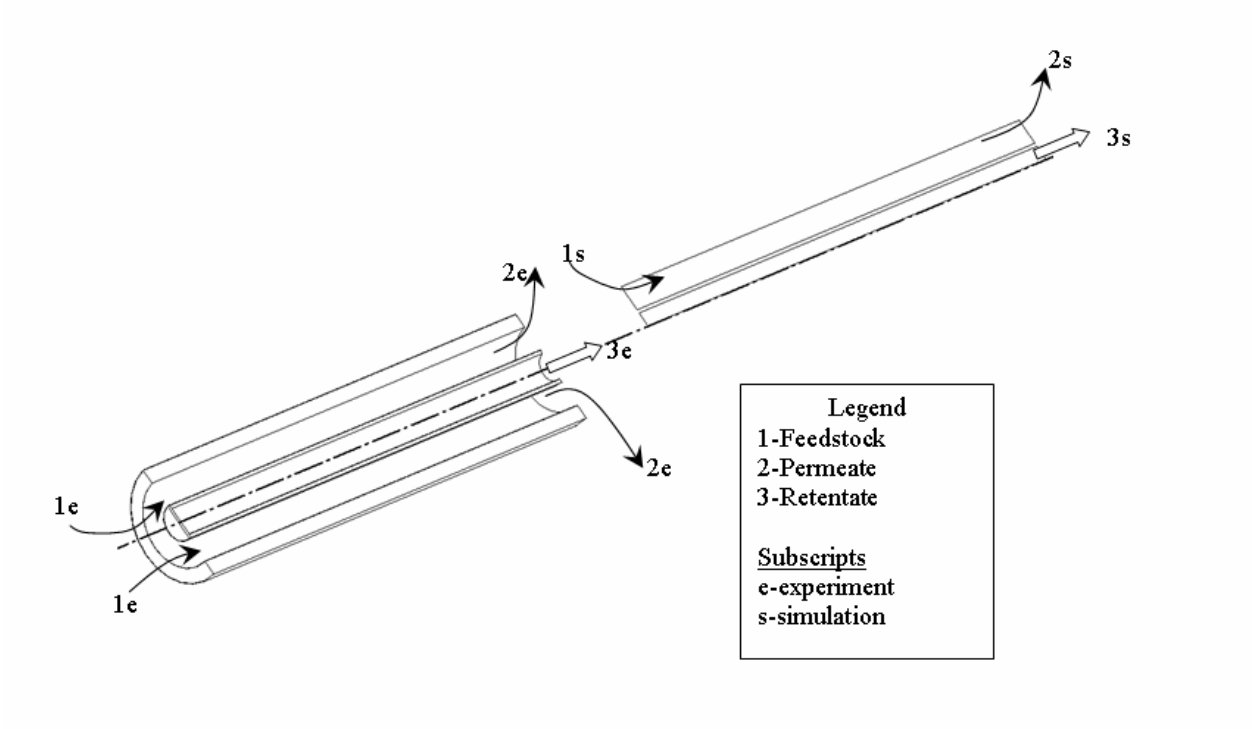

Figure 1 Schematic of a system to separate gases

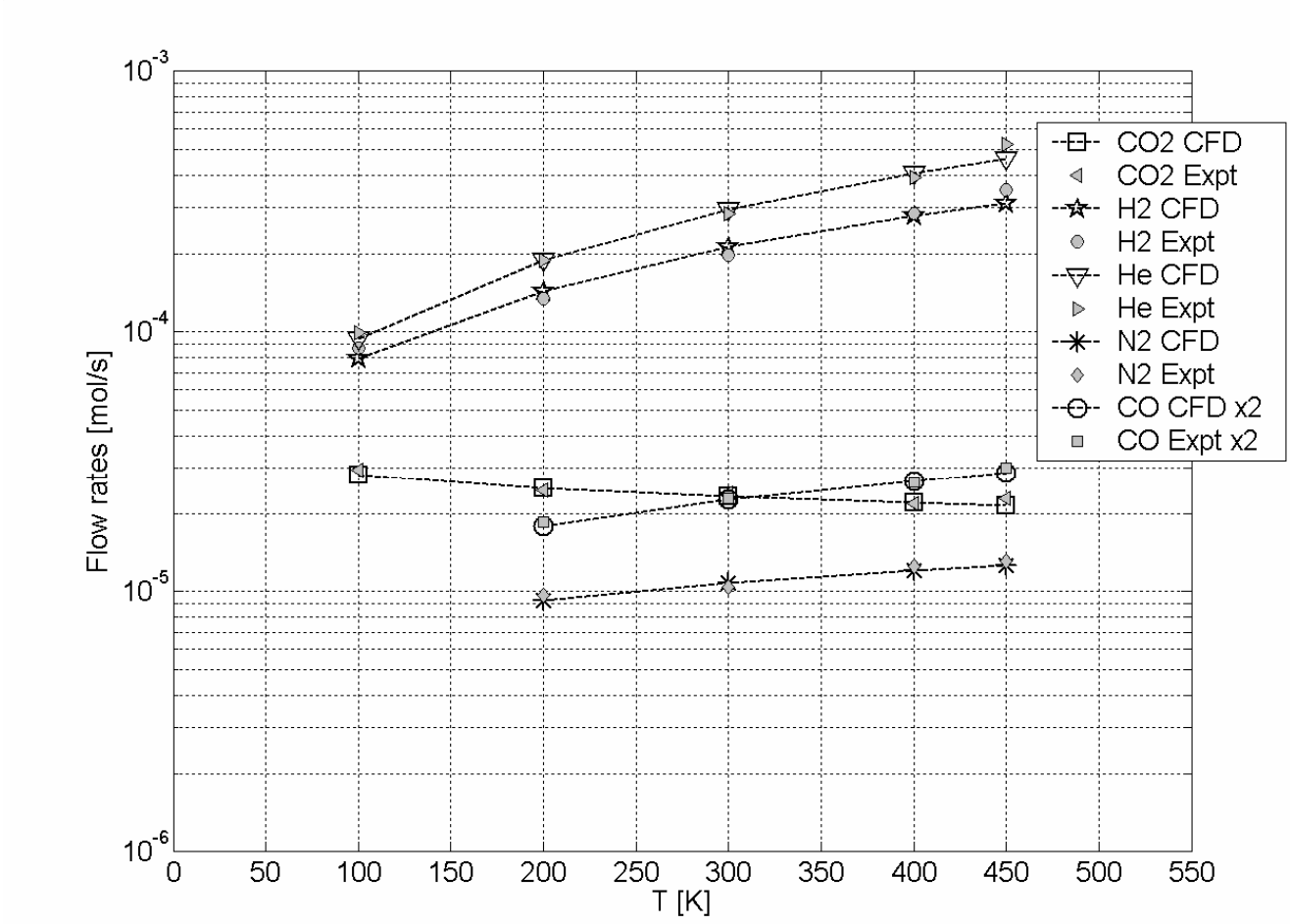

Figure 2 Comparison of flow rates from single gas simulations with experimental measurements (Note CO flow rate multiplied by 2 to separate CO curves from N2 curves on the graph)

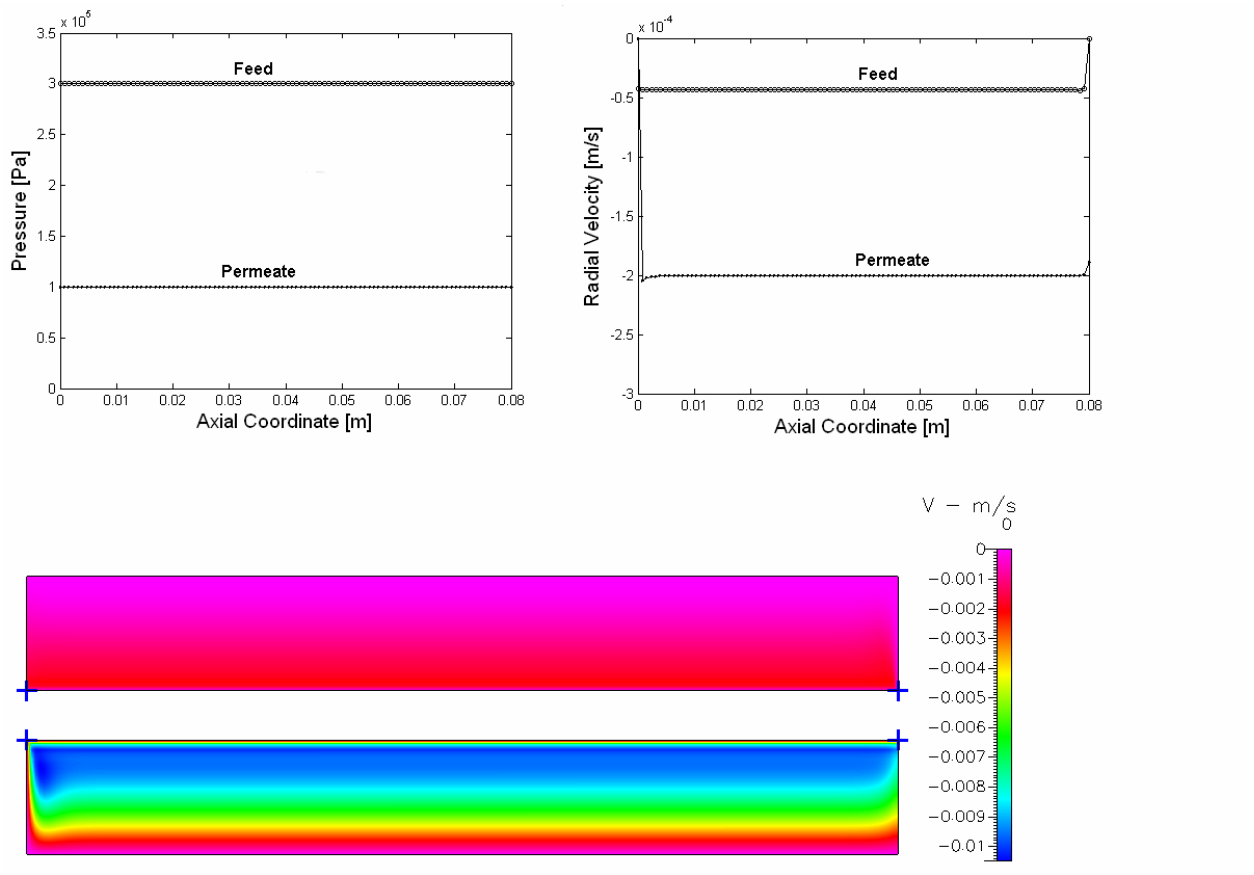

Figure 3 (Lower) Radial velocity field. (Upper) Pressure and Radial velocity as a function of axial coordinate. Simulation for pure H2 flow at 400°C. Flowfield stretched in the radial direction by a factor of 3 for better visibility.

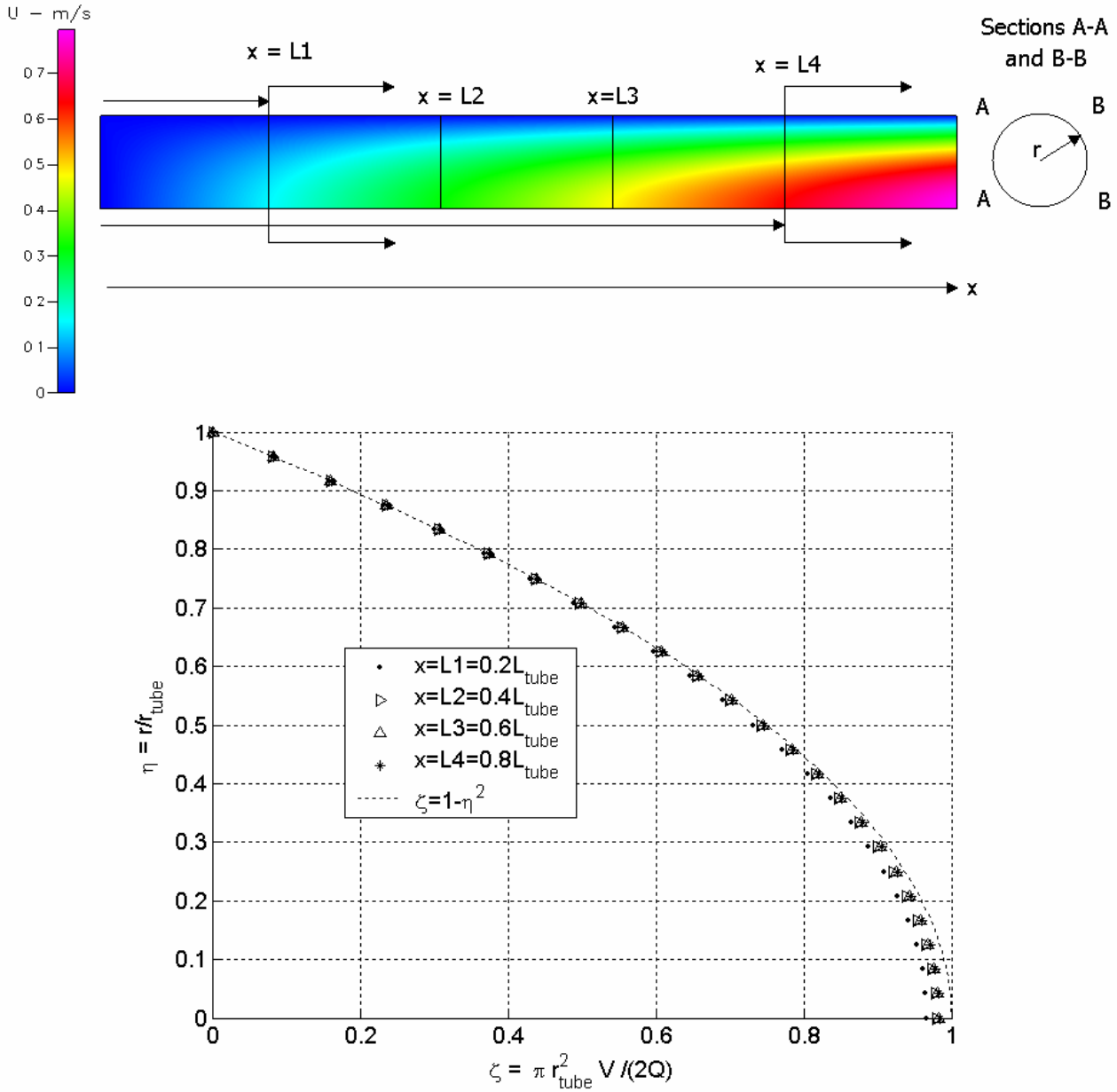

Figure 4 Axial velocity distributions as a function of radial coordinate on the sink side. Simulation for pure H_2 flow at 400°C.

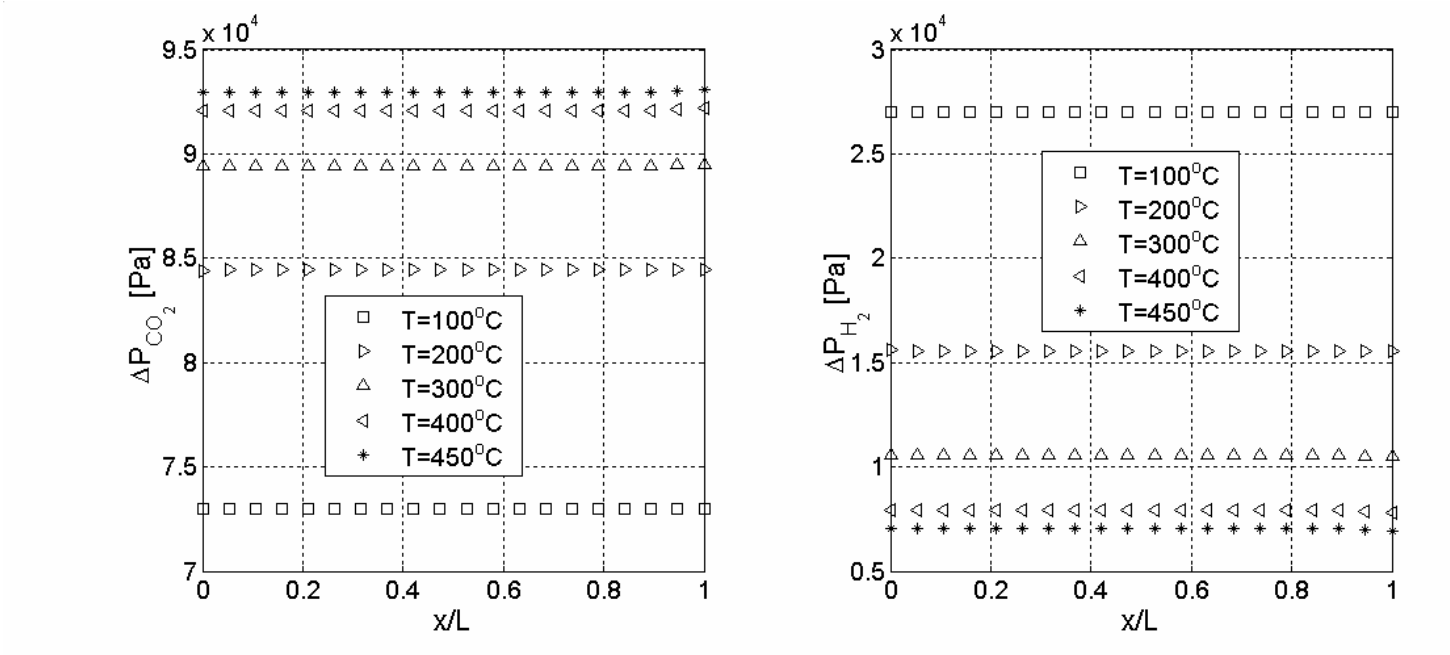

Figure 5 Partial pressure differences ΔP_i across the membrane along the normalized axial coordinate, for mixed gas simulations (CO_2/H_2)